Excited state dynamics of 3,6-diaryl-1,2,4,5-tetrazines. Experimental and theoretical studies

ARTICLE *in* JOURNAL OF PHOTOCHEMISTRY AND PHOTOBIOLOGY A CHEMISTRY · APRIL 2012

Impact Factor: 2.5 · DOI: 10.1016/j.jphotochem.2011.10.025

Journal of Photochemistry and Photobiology A: Chemistry 234 (2012) 12–20

Contents lists available at SciVerse ScienceDirect

Journal of Photochemistry and Photobiology A: Chemistry

journal homepage: www.elsevier.com/locate/jphotochem

Excited state dynamics of 3,6-diaryl-1,2,4,5-tetrazines. Experimental and theoretical studies

Marcel Plugge[a], Valérie Alain-Rizzo[b], Pierre Audebert[b], Albert M. Brouwer[a,*]

[a] University of Amsterdam, van 't Hoff Institute for Molecular Sciences, P.O. Box 94157, 1090 GD Amsterdam, The Netherlands
[b] P.P.S.M., UMR 8531, Ecole Normale Supérieure de Cachan, 61 Av. du Pt Wilson, 94235 Cachan, France

ARTICLE INFO

Article history:
Available online 6 January 2012

Keywords:
Fluorescence
Nonradiative decay
Femtosecond transient absorption
Time-dependent density functional theory

ABSTRACT

The photophysical behavior was studied of three symmetrical 1,2,4,5-tetrazine derivatives substituted with two aromatic substituents (phenyl: **DPT**; *p*-methoxyphenyl: **DAT**; thiophen-2-yl: **DTT**). The UV–visible absorption spectra of these compounds in cyclohexane and acetonitrile show two absorption maxima at 500–550 nm and 290–330 nm, as well as a shoulder at lower energies on the latter absorption band. The electronic transitions were assigned on the basis of TD-DFT calculations. In contrast with some other tetrazine derivatives, these compounds exhibit only weak fluorescence ($\Phi_f \approx 10^{-4}$ to 10^{-3}) from the S_1 ($n\pi^*$) state. When the molecules are excited to a higher energy $\pi\pi^*$ state, fluorescence from the *n*th excited state ($n = 6$ for **DPT**, $n = 5$ for **DAT** and $n = 4$ for **DTT**) is detected. Time-correlated single photon counting (TC-SPC) and femtosecond transient absorption (fs-TA) measurements showed that internal conversion from the S_n state to the S_1 state is unusually slow, of the order of 30 ps for **DTT** and 20 ps for **DAT**.

1. Introduction

1,2,4,5-Tetrazine is a heterocyclic molecule, which consists of an electron poor aromatic ring with four nitrogens. Tetrazines are interesting compounds that can be used as strong electron acceptors, since they have a relatively high reversible reduction potential because of the four electronegative nitrogen atoms in the aromatic ring [1]. Therefore, the excited states of tetrazines are good oxidants, which opens several applications for these molecules, especially including the development of original aromatic hydrocarbon sensors [2]. As the synthesis of 3,6-subsituted tetrazines is rather straightforward [3], they can readily be implemented in various functional molecular systems, such as polymers in which tetrazine derivatives are coupled to electron-rich thiophene groups [4–7]. Tetrazine derivatives have also been frequently used as bridging ligands in metal complexes in which they facilitate metal-metal interactions [8,9] or in switchable metal complexes [10].

Tetrazine derivatives have a low energy absorption band in the visible region, which is weakly influenced by the nature of the substituents [5,11]. In many cases, the first excited state has a very long decay time, involving a forbidden n–π^* transition, in the range 10–160 ns [1]. Therefore, these derivatives are potentially interesting candidates for use in energy transfer cascades, making them, for example, useful building blocks in solar cells [5]. The absorption band of this transition is vibrationally resolved; the vibronic absorption bands at room temperature in the vapor phase of the generic H,H-tetrazine and its infrared spectrum have been studied in the literature [12,13]. Moreover, the vibrational modes that appear in the first absorption band and in the emission band of 3,6-diphenyltetrazine could be assigned with low temperature measurements in cyclohexane [14].

Many tetrazines are known to be fluorescent, although a few of them, like the parent H,H-tetrazine and 3,6-dimethyltetrazine, are not photostable [15–18]. Increasing the size of the substituents improves their photostability, especially when going to aromatics: when one benzene ring is introduced, the photostability is increased by a factor of 30 [18]. However, aromatic substituents also strongly reduce the fluorescence of tetrazines, which is not yet completely understood. Finally, bisaryl tetrazine derivatives also have a well-defined linear structure, which makes this kind of molecules suitable candidates for building rod-shaped multi-chromophore functional systems [19,20].

In the present work, three tetrazine derivatives bearing aromatic groups as substituents, of different nature and different electron donating character, have been studied (Scheme 1).

In this work we focus on the photophysical properties of these three molecules. We present a comparative study of the experimental absorption spectra with time-dependent density functional theory (TD-DFT) calculations. We analyze the properties of **DTT** and **DAT** in comparison with those of **DPT**, which have mostly already

* Corresponding author. Tel.: +31 205255491.
E-mail address: a.m.brouwer@uva.nl (A.M. Brouwer).

1010-6030/$ – see front matter © 2012 Elsevier B.V. All rights reserved.
doi:10.1016/j.jphotochem.2011.10.025

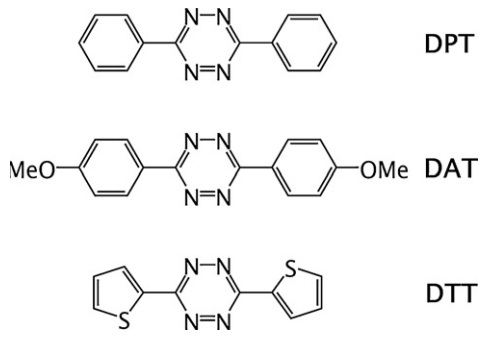

Scheme 1. Tetrazine derivatives studied: **DPT** (3,6-diphenyltetrazine), **DAT** (3,6-di(*p*-methoxyphenyl)tetrazine or 3,6-di(*p*-anisyl)tetrazine) and **DTT** (3,6-di(thiophen-2-yl)tetrazine).

been reported in the literature [14,21]. To understand the excited state dynamics we have performed time resolved fluorescence and femtosecond transient absorption measurements.

2. Experimental

2.1. Synthesis

The three tetrazines described have been prepared according to a recent literature procedure based on the Pinner synthesis, modified by sulfur addition [11], and have spectroscopic data identical to those reported [1,21–23].

2.2. Computational methods

The quantum-chemical calculations have been performed with Gaussian 09 [24]. All calculations were performed using the B3LYP/6-311+G(d) method with the Polarizable Continuum Method to account for solvent effects. Vibrational frequency calculations were performed and the absence of imaginary frequencies showed that the planar structures were true energy minima.

2.3. UV–vis and fluorescence spectroscopy

The UV–vis absorption spectra were recorded on a double beam Varian Cary 3E spectrophotometer, spectral range 190–900 nm with bandwidths down to 0.2 nm. The spectra were recorded in rectangular 10 mm quartz cuvettes. The fluorescence excitation and emission spectra were recorded on a Spex Fluorolog 3 spectrometer, equipped with double grating monochromators in the excitation and emission channels. The excitation light source was a 450 W Xe lamp and the detector a Peltier cooled Hamamatsu R636-10 photomultiplier tube. To obtain a moderate signal-to-noise ratio, the slit in the excitation channel was set at a bandpass of 7 nm, the slit in the emission channel at 4 nm, and relatively long integration times of 3 s per point (increment 1 nm) were used. For comparison: typical settings for routine emission measurements of brightly fluorescent molecules ($\Phi_F \geq 0.3$) with excellent S/N ratio is a slit width in both channels of 2 nm and an integration time of 0.5 s per point. The fluorescence spectra were corrected for the wavelength response of the detection system. For the measurement of quantum yields, a perylenedicarboximide ($\Phi_F = 0.99$) [25] was used as a reference. In order to overcome the large difference in emission intensities of sample and reference, the reference signal was attenuated using a calibrated neutral density filter in the excitation channel. Fluorescence decay times were measured using time correlated single photon counting (TC-SPC) ($\lambda_{exc.} = 323$ nm from a frequency-doubled cavity-dumped DCM dye layer) on a set-up that has been described elsewhere [26]. Decay curves were fitted (Igor Pro 6.0, Wavemetrics) to a sum of exponentials, convolved with the instrument response function. The latter was obtained using Raman scattering of water.

2.4. Femtosecond transient absorption spectra

Femtosecond transient absorption spectra were obtained using a setup in our laboratory [27]. The laser system is based on a Spectra Physics Hurricane Ti-sapphire regenerative amplifier system. The optical bench assembly of the Hurricane includes a seeding pump laser, a pulse stretcher, a Ti-sapphire regenerative amplifier, a Q-switched pump laser and a pulse compressor. The output of the laser is at 800 nm (fwhm = 130 fs) at a repetition rate of 1 kHz. The pump probe setup employed a full spectrum setup based on an optical parametric amplifier (Spectra-Physics OPA) as a pump source. The residual fundamental light (150 μJ/pulse) from the pump OPA was used for the generation of white light. The OPA was used to generate excitation pulses at 323 nm (fourth harmonic signal of the OPA). The polarization of the pump light was controlled by a Berek Polarization Compensator (New Focus). The Berek-polarizer was always included in the setup to provide magic angle conditions. The probe light was passed over a delay line (Physik Instrumente, M-531DD) that provided an experimental time window of 2.5 ns with a maximum resolution of 0.6 fs/step. The white light generation was accomplished by focusing the fundamental (800 nm) into a calcium fluoride plate. The angle between the pump and the probe beam was typically 7–10°. Samples were prepared in a quartz cuvette (l = 2 mm) to have an optical density of 2.0 at the excitation wavelength and were stirred with a "stirring finger" to avoid heating and sample decomposition by the laser beams. The probe beam was coupled into a 400 μm optical fiber after passing through the sample, and detected by a CCD spectrometer (Ocean Optics, PC2000). A chopper, placed in the excitation beam, provides I or I_0 depending on its status (open or closed). Typically, 2000 excitation pulses were averaged to obtain the transient at a particular delay time. Due to wavelength dependence of the speed of light in a medium with refractive index $n > 1$ there is a difference in arrival times of ~1 ps between the blue and red components of the white light (chirp). A polynomial correction for the chirp was used in the global analysis of the datasets, which was performed using the TIMP package [28] with the graphical interface program Glotaran, version 1.0.1 (http://glotaran.org).

3. Results

3.1. UV–vis absorption

The absorption spectra of the three tetrazine derivatives have been measured in cyclohexane (cHex) and acetonitrile (ACN). The normalized spectra are shown in Fig. 1; absorption maxima are listed in Table 1. In the range from 270 to 600 nm, two absorption maxima are present in the spectrum of DPT (Fig. 1A): one maximum is at 558 nm in cHex and a second maximum is at 297 nm. Additionally, a shoulder can be seen around 360 nm. The molar absorption coefficient of the low-energy band has been reported to be ~625 $L\,mol^{-1}\,cm^{-1}$ [14]. The absorption at 297 nm is ~80 times stronger. In comparison to the spectra in cHex, the lowest energy absorption band is blue-shifted in ACN to 543 nm. Despite the absence of a permanent dipole moment, tetrazines are slightly solvatochromic [29].

The shapes of the absorption spectra of **DAT** and **DTT** are very similar to that of **DPT** (Fig. 1B). The position of the maximum of the visible absorption peak in cHex of **DAT** (558 nm) is comparable to that of **DPT** (556 nm), while that of **DTT** (536 nm) is at shorter wavelengths. This is also the case in ACN. The absorption peaks between 300 and 350 nm of **DAT** (342 nm) and

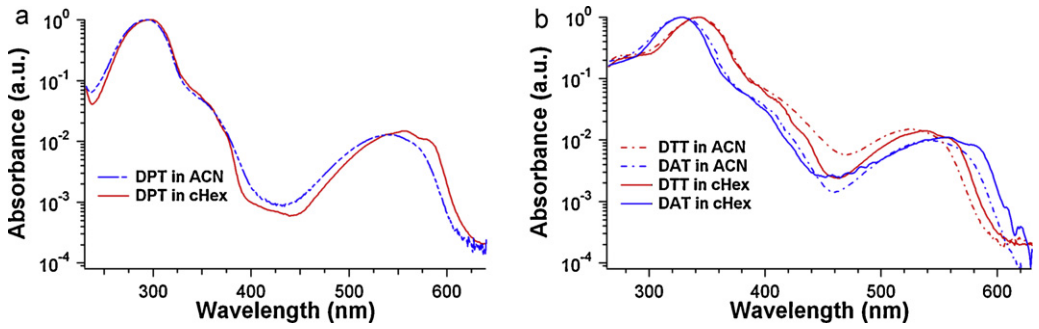

Fig. 1. (A) Normalized absorption spectra of **DPT** in cyclohexane (red) and in acetonitrile (blue). (B) normalized absorption spectra of **DAT** (blue) and **DTT** (red) in cyclohexane (solid lines) and in acetonitrile (dashed lines). (For interpretation of references to color in this figure legend, the reader is referred to the web version of this article.)

DTT (343 nm) are red shifted compared to the corresponding band of **DPT** (297 nm). The UV band is ~70 times stronger than the visible absorption. In all three compounds, a shoulder is present on the low-energy side of this absorption band. The extent of the blue shift induced by the solvent of the lowest-energy absorption peak is similar for the three molecules. The strong UV absorption is not solvatochromic.

3.2. Computation of ground state geometries and orbitals

The electronic structures of compounds **DPT**, **DAT** and **DTT** have been analyzed using quantum chemical calculations. Firstly, the geometry of the molecules and the molecular orbitals have been calculated using the B3LYP hybrid density functional method with the 6-311 + G(d) basis set and the Polarizable Continuum Model (PCM) solvent model for ACN or cHex. The geometry of **DPT** has D_{2h} symmetry with the phenyl rings in the same plane as the tetrazine ring, in accordance with its crystal structure [23]. The geometries of **DAT** and **DTT** are also planar (C_{2h} or C_{2v}). Secondly, based on the optimized geometries, the optical transition energies and oscillator strengths were calculated using TD-DFT calculations with the same basis set. The orbital energies of these molecules are shown in Fig. 2A. Similar orbitals are connected with lines. Also representations of five relevant orbitals of **DPT** and **DTT** are shown in Fig. 2B and C.

The order of occupied molecular orbitals of **DAT** and **DTT** is different from that of **DPT**. First the five highest occupied molecular orbitals (HOMOs) are described: the highest occupied molecular orbital (HOMO) in **DPT** is made of the non-bonding lone pairs of the nitrogens in the tetrazine ring (*n*-orbitals); this orbital is depicted in green in Fig. 2A. The HOMO-1, depicted in red, the π-orbital delocalized over the three aromatic rings, lies close in energy. The HOMO-2 and HOMO-3 of **DPT**, depicted in blue, are the essentially degenerate symmetrical and anti-symmetrical π-orbitals localized on the phenyl rings. Lastly, the HOMO-4 of **DPT** is a π-orbital spread over the three rings, similar to the HOMO-1.

The π-orbitals on the tetrazine that are mixed with the π-orbitals of the substituents are higher in energy when the aromatic

Table 1
Calculated and experimental excitation energies, and calculated oscillator strengths and leading configurations[a] for low-energy allowed singlet–singlet transitions of tetrazines in cyclohexane and acetonitrile.

k[b]	Transition	Pol.[c]	cHex				ACN			
			TD-DFT		Exp.		TD-DFT		Exp.	
			eV	nm	*f*[d]	nm	eV	nm	*f*[d]	nm
DPT										
1	HO → LU	*z*	2.10	590	0.0042	558	2.13	582	0.0041	543
2	HO → LU + 1		2.85	434	0.0000		2.92	425	0.0000	
3	HO-1 → LU	*y*	3.15	394	0.0059		3.10	400	0.0056	
4	(HO-2 → LU) – (LU + 1 → HO-1)	*x*	3.61	343	0.0469		3.56	349	0.0133	
5	HO-3 → LU		3.65	340	0.0000		3.58	346	0.0000	
6	(HO-2 → LU) + (HO-1 → LU + 1)	*x*	3.78	328	1.1997	297	3.77	329	1.2061	293
DAT										
1	HO-1 → LU	*z*	2.10	590	0.0041	556	2.13	583	0.0041	545
2	HO → LU	*y*	2.67	465	0.0029		2.58	481	0.0027	
3	HO-1 → LU + 1		2.96	419	0.0000		3.03	409	0.0000	
4	HO-2 → LU		3.22	385	0.0011		3.12	397	0.0001	
5	(HO-4 → LU) + (HO → LU + 1)	*x*	3.38	367	1.3403	342	3.35	370	1.306	343
6	(HO-4 → LU) – (LU + 1 → HO-2)		3.83	324	0.0005		3.75	330	0.0003	
DTT										
1	HO-1 → LU	*z*	2.21	562	0.0046	536	2.24	553	0.0045	526
2	HO → LU	*x*	2.75	451	0.0092		2.67	464	0.0084	
3	HO → LU + 1		2.90	427	0.0000		2.99	415	0.0000	
4	(HO-4 → LU) + (HO → LU + 1)	*y*	3.30	376	0.9787	329	3.29	377	0.9076	323
5	(HO-2 → LU) + (LU → HO-4)		3.51	353	0.0000		3.42	362	0.0000	
6	(HO-2 → LU) + (HO-4 → LU)		3.64	340	0.0000		3.57	348	0.0000	
7	(HO-4 → LU) – (LU + 1 → HO-1)	*y*	3.65	339	0.1603		3.58	346	0.2113	

[a] HO = highest occupied molecular orbital; LU = lowest unoccupied molecular orbital.
[b] *k* = number of excited state according to the TD-DFT calculations.
[c] Pol. = polarization; for all molecules the *z*-axis is orthogonal to the plane; for **DPT** and **DAT** the *x*-axis corresponds to the long axis of the molecule, for **DTT** it is along the short axis.
[d] *f* = oscillator strength.

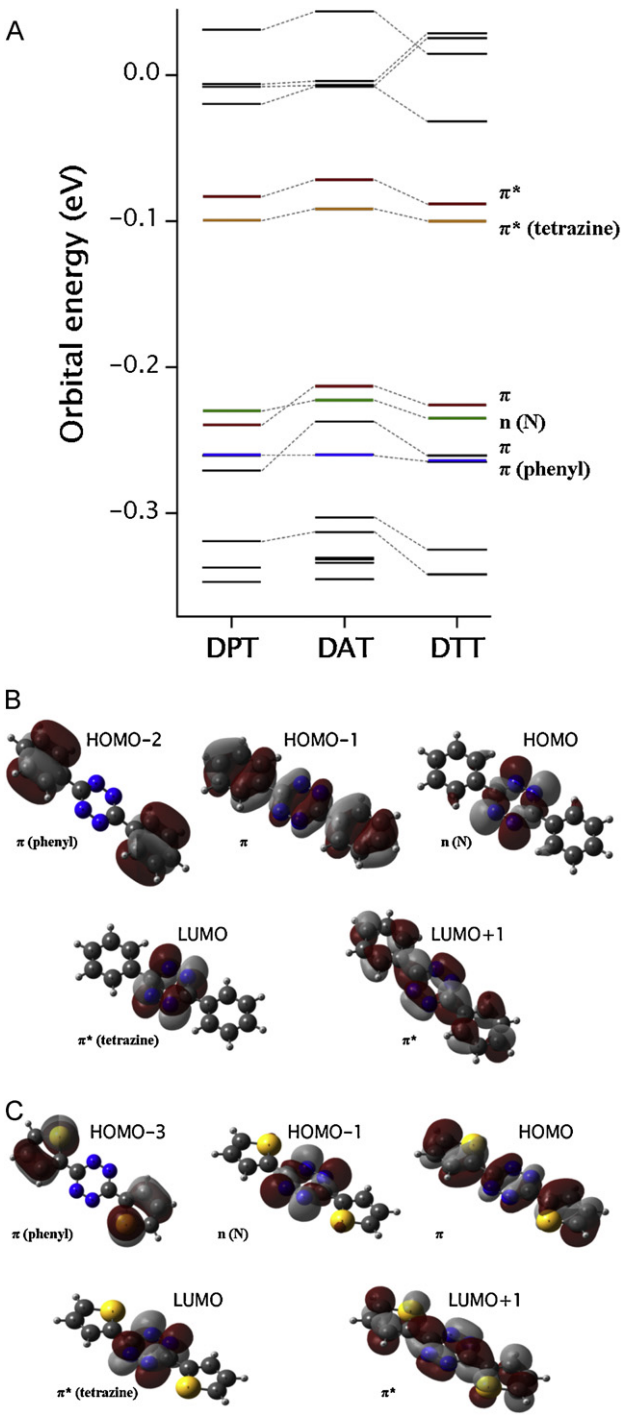

Fig. 2. (A) Calculated orbital energies of **DPT**, **DAT** and **DTT** in cyclohexane. Colored lines connected with dotted lines represent similar orbitals. (B) Plots of calculated orbitals of **DPT**. (C) Plots of calculated orbitals of **DTT**. Note the reversal of HOMO-1 and HOMO as compared to **DPT**. (For interpretation of references to color in this figure legend, the reader is referred to the web version of this article.)

substituents are more electron rich, which is the case in **DAT** and **DTT**. As a result, the π-orbitals over the three aromatic rings are the HOMO instead of the *n*-orbitals on the tetrazine ring. This inversion of ordering of orbitals has also been calculated for other tetrazine derivatives with electron rich substituents [1]. Likewise, the orbital that is the HOMO-4 for **DPT** becomes relatively higher in energy, thus becoming the HOMO-2 for **DAT** and **DTT**.

For all three molecules, the lowest unoccupied molecular orbital (LUMO; orange in Fig. 2A) is a π* orbital situated only on the tetrazine ring. At somewhat higher energies the LUMO + 1 is found, depicted in red, which is a π* orbital delocalized over the three aromatic rings.

Changing the solvent from cHex to ACN slightly changes the relative energies of the orbitals, but not their relative positions with respect to each other.

The results from our calculations on **DTT** disagree somewhat with similar DFT studies from other groups who used a different basis set (6-31G*) and performed the DFT calculations in vacuum [30]. In Ref. [30], the order of the orbitals differs from our results: in our calculations, the HOMO and HOMO-1 of **DTT** are inverted compared to **DPT**, whereas according to Kurach et al. this is not the case. Moreover, these authors state that for **DTT**, and incidentally also for **DPT**, that π* orbitals on the tetrazine ring are the LUMO + 1, while in our calculation this is the LUMO for all three studied molecules. Other publications on **DPT** and on other tetrazine derivatives confirm that this particular orbital is the LUMO, regardless of the type of substituent.

3.3. TD-DFT calculations: transition energies and oscillator strengths

The results of the TD-DFT calculations on **DPT** agree rather well with TD-DFT calculations in vacuum that are known in the literature [21]. The calculated UV–vis spectrum is also in good qualitative agreement with the experimental data, i.e., the three optical transitions that are observed in the absorption spectra in the range 270–600 nm could be properly reproduced. The calculated transitions and the experimental values are included in Table 1. Using the results of TD-DFT calculations, the three main absorption transitions in the UV–vis spectra in the visible region can be properly assigned. The orbitals involved in each optically allowed transition are the same for all molecules. The leading configuration of the first excited state is an *n*-π* transition (S_0–S_1) from the nonbonding orbitals of the nitrogens (HOMO) in **DPT** to the antibonding π* orbitals of the tetrazine ring (LUMO). Since this is a forbidden transition, the oscillator strength is low. This is in agreement with the experimental results where this absorption band is rather weak. Also in **DAT** and **DTT**, the *n*-π* transition (HOMO-1 → LUMO) is the lowest in energy. Interestingly, while the relative orbital levels of **DTT** are in disagreement, the TD-DFT calculations reported in Ref. [30] do agree in terms of the orbitals involved in this transition and those in the transition in the range 300–350 nm.

The second transition that is distinguished in the experimental spectra is a weak π–π* transition around 400 nm from π-orbitals that are delocalized over the molecule (HOMO-1 → LUMO for **DPT**; HOMO → LUMO for **DTT** and **DAT**). Actually, an intermediate transition of **DPT** is calculated which involves an *n*–π* transition (HOMO → LUMO + 1) with oscillator strength of 0. Such transitions have also been calculated in the literature for **DPT** and tetrazine derivatives with pyridine as substituent [21]. This transition is present for **DAT** and **DTT** as the third transition. Regarding the energy of the excited state corresponding to the shoulder on the strong UV absorption band, there is a discrepancy between the calculations and the experimental data. For **DAT** and **DTT**, this transition should be around 460–480 nm according to the calculations, whereas in the experimental data the shoulder is observed at 400 nm.

Lastly, the absorption band in the range 300–350 nm arises from a combination of essentially two π–π* transitions: primarily from the orbitals on the tetrazine ring and secondly from the orbitals on the substituents. In the UV–vis spectra, this transition gives rise to the most intense absorption of the molecules at λ > 270 nm. The calculated oscillator strength of this transition is indeed more than a factor 100 larger than that of the first transition. The energy of this transition strongly depends on the properties of the substituents,

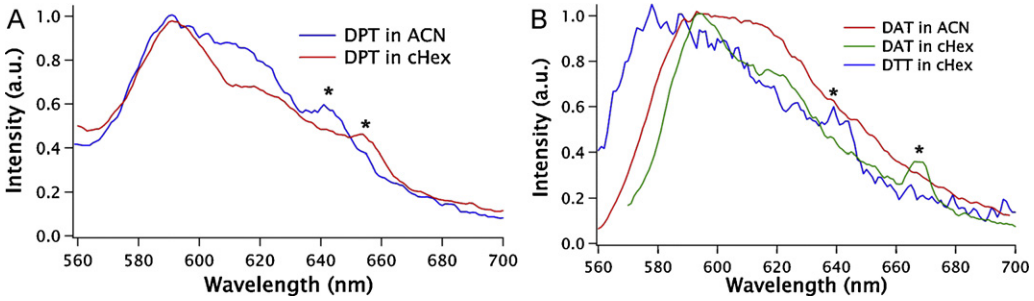

Fig. 3. (A) Normalized emission spectra of **DPT** in acetonitrile ($\lambda_{exc.}$ = 550 nm, blue line) and in cyclohexane ($\lambda_{exc.}$ = 540 nm, red line). (B) normalized emission spectra of **DAT** in acetonitrile ($\lambda_{exc.}$ = 540 nm, red line) and in cyclohexane ($\lambda_{exc.}$ = 560 nm, green line) and of **DTT** in cyclohexane ($\lambda_{exc.}$ = 540 nm, blue line). Concentrations were ~10^{-3} M in all cases. The peaks marked with * are due to Raman scattering of the solvent. (For interpretation of references to color in this figure legend, the reader is referred to the web version of this article.)

and also the number of this transition varies depending on the substituent: in **DPT** this state is the sixth excited state whereas in **DAT** it is the fifth, and in **DTT** the fourth. Since the nature of this excited state is the same for each molecule, it will in the remainder of the paper be called the S_n state, where $n = 6$ for **DPT**, $n = 5$ for **DAT** and $n = 4$ for **DTT**.

The observed blue shift in the n–π^* absorption bands due to the increased polarity of the solvent is successfully reproduced by the calculations.

3.4. Emission spectra

Upon excitation at the first absorption maximum ($\lambda_{exc} \approx 550$ nm) of **DPT**, very weak fluorescence is observed in the region 600–750 nm ($\Phi_f \approx 1.5 \times 10^{-4}$ in cyclohexane). This is in line with earlier studies on this molecule [14]. The normalized emission spectra are shown in Fig. 3; the spectra are still noisy despite the use of wide spectrometer slits and relatively long integration time (See Section 2). The Raman scattering peak of the solvent, which is typically 3000 cm^{-1} at lower energy than the excitation light is visible in the emission spectra at 645 nm (for $\lambda_{exc.}$ = 540 nm), 660 nm (for $\lambda_{exc.}$ = 550 nm) or 675 nm (for $\lambda_{exc.}$ = 560 nm). Appreciable fluorescence has been observed for other tetrazine derivatives where inversion of orbitals takes place [1]. However, for **DAT** and **DTT**, the fluorescence quantum yield is hardly higher than for **DPT**. For **DAT** we find $\Phi_f \approx 10^{-3}$ in cHex and $\Phi_f \approx 1.3 \times 10^{-3}$ in ACN. For **DTT** in cHex $\Phi_f \approx 5.9 \times 10^{-4}$. For **DTT** in ACN, the fluorescence was so weak that a quantum yield could not be estimated.

The compounds **DAT** and **DTT** were further studied with excitation at their second absorption maxima ($\lambda_{exc.} \approx$ 320–340 nm), which leads to a higher excited S_n state. An identical emission spectrum from the S_1 state is obtained, but additionally, emission in the region 370–430 nm is observed which is attributed to emission from the S_n state. The emission spectra of **DAT** and **DTT** are shown in Figs. 4 and 5, respectively. They are normalized at the emission peak of the S_1 emission. In the spectra, the Raman scattering of the solvent is obviously present around 350 nm (for $\lambda_{exc.}$ = 320 nm) or 380 nm (for $\lambda_{exc.}$ = 340 nm). For comparison, the low-energy absorption bands of the samples are shown in green in the graphs.

3.5. Fluorescence lifetime measurements

The fluorescence lifetimes of **DTT** and **DAT** were measured with the TC-SPC setup in both cHex and ACN, using $\lambda_{exc.}$ = 323 nm and $\lambda_{det.}$ = 600 nm. With this excitation energy, the molecules are excited to the S_n state, and we detect the fluorescence from the S_1 state. The fluorescence decay curves could be properly fitted when a rise time of about 15 ps was taken into account (Fig. 6). This value is close to the system response of the measurement system (full width at half maximum ~17 ps) and there may thus be some uncertainty in its precise value. The fluorescence decay time is 200–500 ps for **DTT**, and 600–900 ps for **DAT** (Table 2). Due to the very poor fluorescence signal from the sample of **DTT** in ACN, the data could not be fitted very accurately. However, here also a rise is apparent.

3.6. Femtosecond transient absorption spectra

To further understand the occurrence of the S_n emission and the complex fluorescence time profile of the S_1 emission, femtosecond transient absorption measurements were performed on **DAT** and **DTT**. With these measurements, the rate of internal conversion from the S_n state to the S_1 state can be measured with better time resolution than with the fluorescence lifetime measurements. Due to poor solubility in cHex, **DAT** could only be analyzed in ACN. The samples have been excited to their S_n state ($\lambda_{exc.}$ = 323 nm) and the detection range was from 360 nm

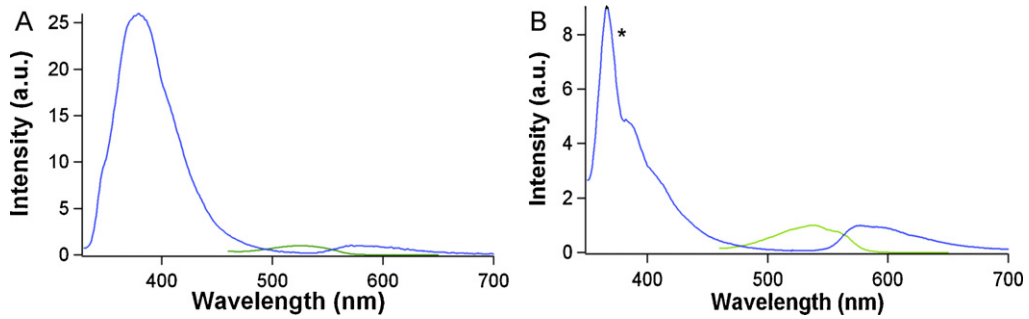

Fig. 4. Normalized emission spectra (blue) of **DTT** (~10^{-5} M) in acetonitrile ((A) $\lambda_{exc.}$ = 330 nm) and cyclohexane ((B) $\lambda_{exc.}$ = 340 nm). The peaks marked with * are due to Raman scattering of the solvent. For comparison, the low-energy absorption bands are shown, normalized to the corresponding emission. (For interpretation of references to color in this sentence, the reader is referred to the web version of this article.)

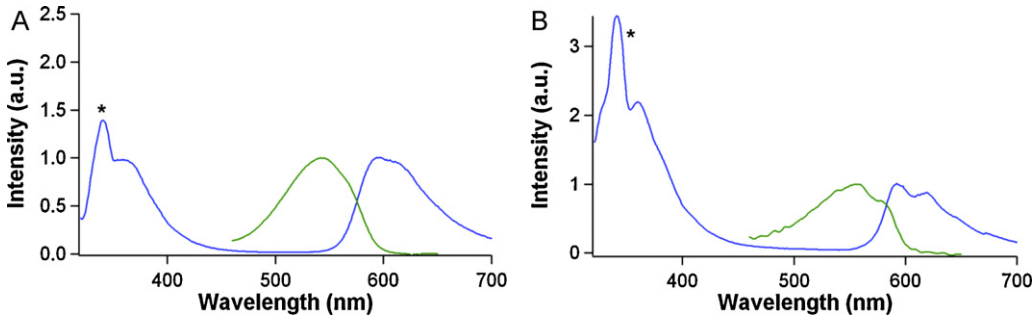

Fig. 5. Normalized emission spectra ($\lambda_{exc.}$ = 320 nm) of **DAT** (~10^{-5} M) in acetonitrile (A) and cyclohexane (B). The peaks marked with * are due to Raman scattering of the solvent. For comparison, the low-energy absorption bands are shown, normalized to the corresponding emission.

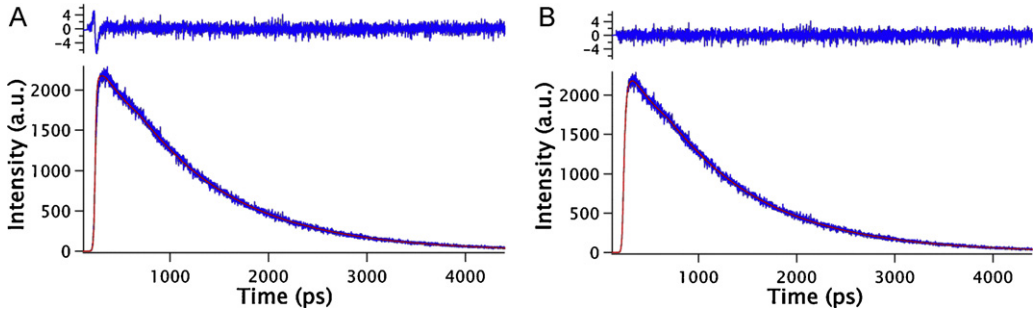

Fig. 6. Fluorescence time profile ($\lambda_{exc.}$ = 323 nm, $\lambda_{det.}$ = 600 nm) of **DAT** in acetonitrile. (A) monoexponential fit; (B) biexponential fit.

Table 2
Fluorescence time constants of **DAT** and **DTT** in acetonitrile and cyclohexane ($\lambda_{exc.}$ = 323 nm, $\lambda_{det.}$ = 600 nm).

Solvent	τ_1 (ps) [b]	τ_2 (ns) [c]	χ^2
DAT			
ACN	15	0.98	0.978
cHex	16	0.59	1.012
DTT			
ACN[a]	8	0.54	0.818
cHex	15	0.28	1.322

[a] Because of very low signal, the fit cannot be considered reliable.
[b] Rise time.
[c] Decay time. Relative amplitudes of the rise and decay are in all cases approximately equal.

to 790 nm. The transient absorption difference spectra of **DTT** in ACN are shown in Fig. 7. The time evolution at certain detection wavelengths is shown in Fig. 8. Datasets were analyzed using global analysis [28]. To interpret the data, a sequential model is used, in which vibrational relaxation of the S_n state, internal conversion from S_n to S_1 and transition from S_1 to the ground state are considered to be the only processes following excitation. With this model,

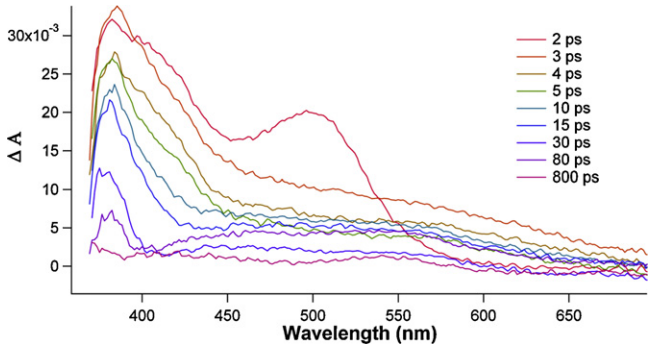

Fig. 7. Transient absorption difference spectra of **DTT** in acetonitrile ($\lambda_{exc.}$ = 323 nm).

the data of all three samples could be fitted reasonably well and the spectra of the components as well as the rates of the fast processes could thus be determined.

The transient absorption difference spectra of the various components obtained with the global fits are shown in panels A–C in Fig. 9 for **DTT** in ACN, **DTT** in cHex and **DAT** in ACN, respectively. The spectrum of **DTT** in ACN directly after excitation (green spectrum in Fig. 9A) shows a broad positive absorption band from 370 to 450 nm. The bleached ground state absorption (<350 nm) falls outside of the detection range. The initial component undergoes vibrational relaxation with a time constant τ_1 of about 1.5 ps, accompanied by narrowing of the spectral features (Table 3). The subsequent conversion of the S_n to the S_1 state is a rather slow process: while usually internal conversion is on a picosecond time scale, a time constant (τ_2) of 20–35 ps was found. The third process, transition of the S_1 state to the ground state, appeared with a lifetime of 1–2 ns. Because of the weak signal at longer time intervals the time constant τ_3 could not be measured accurately, but it is in qualitative agreement with the fluorescence lifetime measured much more reliably with the TC-SPC set up. The S_n state (blue spectrum in Fig. 9A) and the S_1 state (red spectrum in Fig. 9A) have an absorption band in the range 350–450 nm which peaks around 380 nm. In the region 450–570 nm the first two components show a very broad unstructured absorption band, and the last component has two positive absorption bands at 475 nm and 550 nm.

Table 3
Time constants from the transient absorption measurements.

	τ_1 (ps)	τ_2 (ps)	τ_3 (ns)
DTT			
ACN	1.5	29	1.2
cHex	2.6	35	1.4
DAT			
ACN	1.6	20	1.7

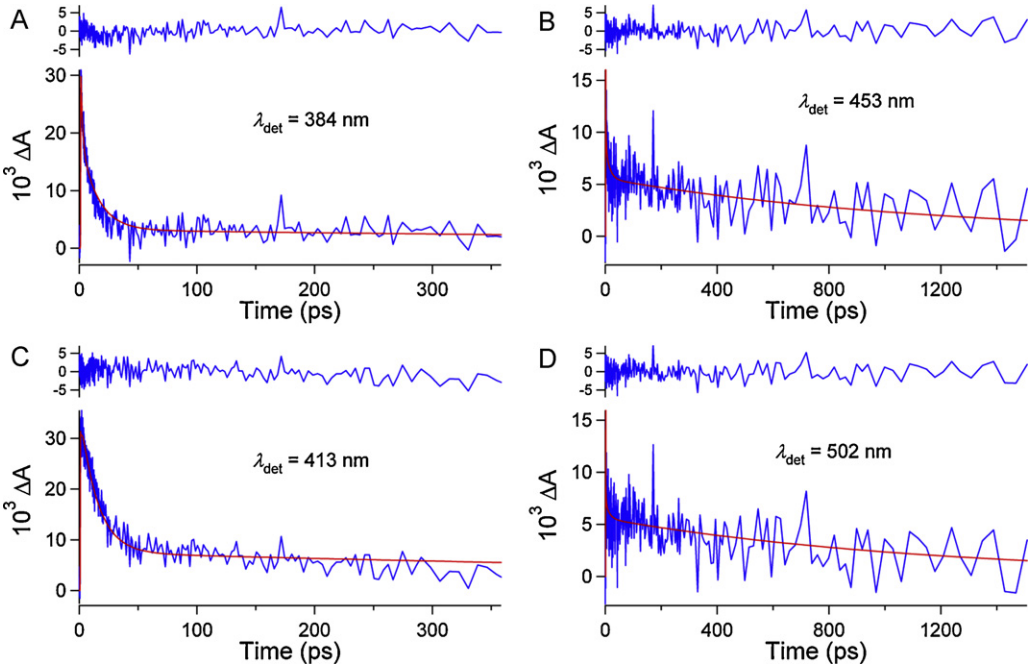

Fig. 8. Time evolution of transient absorption of **DTT** in acetonitrile at selected probe wavelengths.

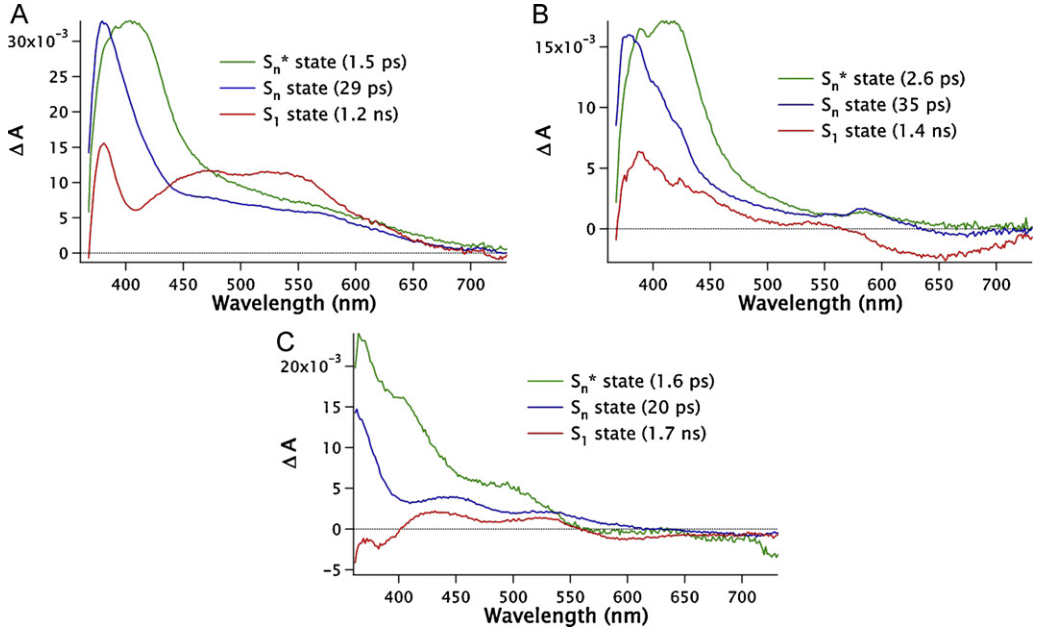

Fig. 9. Evolution associated decay spectra of **DTT** in acetonitrile (panel A), **DTT** in cyclohexane (panel B) and **DAT** in acetonitrile (panel C).

The spectra of the three components of **DTT** in cHex (Fig. 9B) look similar to those in ACN in the range 350–450 nm, but here no obvious absorption above 500 nm is detected. Instead, the S_1 state shows a negative band from 580 to 700 nm, which may be due to stimulated S_1 emission. Compared to **DTT**, the absorption bands of the S_n state and the S_1 state in **DAT** in ACN (Fig. 9C) are shifted to shorter wavelengths. Likewise, here also a negative band is present from 560 to 700 nm, consistent with emission from the S_1 state. The time constants $\tau_1 - \tau_3$ are listed in Table 3. The lifetimes of **DTT** are similar in ACN and cHex. The relatively lower S_n emission compared to S_1 emission for **DAT** compared to **DTT** is consistent with the rate of the internal conversion process of the S_n state to the S_1 state (τ_2) which is faster for **DAT** (20 ps).

4. Discussion

The studied molecules **DPT**, **DAT** and **DTT** have three electronic transitions that can be discerned in the UV–vis spectra in the range 270–600 nm. These transitions could be properly reproduced and assigned by means of TD-DFT calculations. The lowest excited state corresponds to an n–π^* transition (S_0–S_1) from the non-bonding orbitals of the nitrogens to the π^* orbitals of the tetrazine ring. The other two UV bands are due to π–π^* transitions.

Very weak fluorescence from the S_1 state of these molecules is observed. In contrast, tetrazine derivatives with chlorine or methoxy groups as substituents show substantial fluorescence from the S_1 state; for example, dichlorotetrazine has a fluorescence

quantum yield of 0.11 and a fluorescence lifetime of 58 ns [3]. This implies a radiative lifetime of 530 ns, close to the reported value for **DPT** of 660 ns [14]. A large range of substituted tetrazines, with widely varying fluorescence quantum yields, show similar radiative lifetimes [31]. The weak fluorescence of the aromatic substituted tetrazines studied in the present work fits perfectly into this picture. The lifetime of the S_1 emission is <1 ns and the fluorescence quantum yield is $\leq$0.001 [32]. The excited decay times of the S_1 state are longer for **DAT** than for **DTT**, and longer in acetonitrile than in cyclohexane. The emission quantum yields are all low, and were not measured accurately in the present work, but they clearly follow the same trend (fig. 3).

Upon excitation to the S_n state, the molecules show dual emission, not only from the S_1 state but also from the higher-energy S_n state. This emission is significant and in most cases even stronger than the S_1 emission in the steady state fluorescence measurements. Based on the energy gap law, relaxation from the S_n to the S_1 state can be expected to be a relatively slow process [33]. Thus, radiative decay from the S_n state may compete with internal conversion to the S_1 state, also since the oscillator strength of the S_0–S_n transition is a factor 100 larger than that of S_0–S_1. It should be noted that TD-DFT calculations show that some states are present between the S_n state and the S_1 state, which should facilitate non-radiative decay via intermediate electronic states with smaller energy gaps. Considering this, it is actually surprising that emission occurs from the S_n state. This higher excited state emission has also been observed for **DPT**, both in our measurements, and in Ref. [14] but it is much weaker than in the cases of **DAT** and **DTT**.

From the time-resolved fluorescence and femtosecond transient absorption measurements, a quantitative picture of the photophysical behavior of the analyzed tetrazine derivatives can be constructed (Fig. 10). From the S_n state the compounds can undergo either internal conversion to the S_1 state or direct emission to the ground state. According to transient absorption, the relaxation from the S_n to the S_1 state is a relatively slow process with time constants of ~20 ps for **DAT** and ~30 ps for **DTT**. This is also observed as a short rise time of the S_1 emission in the fluorescence time profile.

The slow internal conversion is unusual but not unique [34]; for example, azulene has a gap between the S_2 and S_1 states (~14,000 cm^{-1}) similar to that of the studied tetrazine derivatives, and shows S_2 emission due to very slow internal conversion [35,36]. The fluorescence lifetime of this molecule has been determined as 1.6 ns [37]. Likewise, in studies on trans-1,2-diarylethenes, it has been shown that with relatively slow S_2–S_1 conversion, other relaxation pathways become competitive, leading to S_2 emission with lifetimes in the 100–800 ps range [38]. In case of alkoxy-substituted phthalocyanines, weak emission from a higher state along with the S_1 emission is observed; this emission has an unusual long luminescence lifetime and was attributed to ligand-centred triplet states [39]. Other examples of compounds that exhibit (weak) higher excited state emission also show relatively slow relaxation to the S_1 state from the emitting state, but this still is in the order of a few picoseconds [40–42].

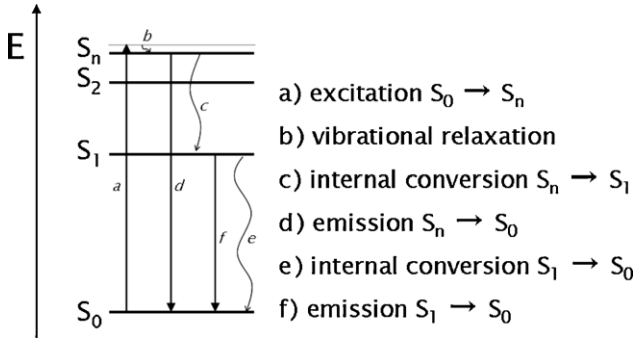

Fig. 10. Photophysical behavior of the tetrazine derivatives.

Returning to the emission from the lowest excited state we note that the large difference between the fluorescence quantum yields of different tetrazine derivatives is rather surprising: the S_1–S_0 decay involves the same forbidden n–π^* transition independent of the substituents. It has been observed that the orbital ordering is important in determining the fluorescence efficiency of substituted tetrazines: when the HOMO is calculated to be an n-orbital, fluorescence is efficient, when it is a π-orbital fluorescence is weak or absent [31]. The case of **DPT** studied in the present paper appears to be an exception to this rule. The n–π^* state, however, is invariably the lowest excited state of tetrazines, regardless of their emission efficiency, and regardless of the orbital ordering. The emission quantum yield is not controlled by the radiative process, but completely determined by the as yet unknown nonradiative decay pathway. Therefore, we propose that the orbital ordering is correlated with the ordering of excited states of higher energy than the n–π^* state, which are probably involved in the nonradiative decay channel. In particular, a high-energy π–MO naturally gives rise to a relatively low-energy π–π^* state, which is absent in the highly fluorescent tetrazines. Future quantum-chemical explorations of the excited state energy surfaces will undoubtedly shed light on the efficient nonradiative decay pathway of the weakly fluorescent tetrazines. We note that the decay appears to be directly to the ground state, as no indication for long-lived transient states such as triplet states was observed in the fs-TA measurements.

5. Conclusion

The photophysical properties of three 1,2,4,5-tetrazine derivatives with aromatic substituents have been studied. Their absorption spectra have been compared with TD-DFT calculations, which are in quite good agreement. Very weak fluorescence from the S_1 state is observed, since it involves a forbidden n–π^* transition. The emission quantum yield appears not to be simply related with the nature of the highest occupied MO [3,31], because in **DPT** this is the n-orbital but in **DAT** and **DTT** it is the π–MO.

Fluorescence from the higher-energy S_n π–π^* state is in most cases stronger than the S_1 emission. The excited state decay time of the S_n state is several tens of picoseconds. Based on the large energy gap with S_1 this may seem plausible, but TD-DFT calculations have located several states in between the emitting S_n state and the S_1 state, one of which is also observable in UV absorption. Thus, a sequence of rapid nonradiative decays between electronic states with a small energy gap should be expected, which renders emission from the S_n state a surprising observation.

Acknowledgments

This work was supported within FP6 of the European Union by the ERANET consortium NanoSci-ERA: Nanoscience in the European Research Area, in the context of the MOLIMEN project (MOlecules and LIght in MEtal Nanostructures). We thank Dr. Alberto Marini for discussions about the computational methodology, Michiel Groeneveld for help with the transient absorption measurements and Dr. René M. Williams for assistance with the data analysis.

References

[1] G. Clavier, P. Audebert, s-Tetrazines as building blocks for new functional molecules and molecular materials, Chem. Rev. 110 (2010) 3299–3314.

[2] P. Audebert, C., Allain, L. Galmiche, French Patent Request no. 1061377,2010, France.
[3] P. Audebert, F. Miomandre, G. Clavier, M.C. Vernières, S. Badré, R. Méallet-Renault, Synthesis and properties of new tetrazines substituted by heteroatoms: towards the world's smallest organic fluorophores, Chem. Eur. J. 11 (2005) 5667–5673.
[4] P. Audebert, S. Sadki, F. Miomandre, G. Clavier, First example of an electroactive polymer issued from an oligothiophene substituted tetrazine, Electrochem. Commun. 6 (2004) 144–147.
[5] Z. Li, J.F. Ding, N.H. Song, X.M. Du, J.Y. Zhou, J.P. Lu, Y. Tao, Alternating copolymers of dithienyl-s-tetrazine and cyclopentadithiophene for organic photovoltaic applications, Chem. Mater. 23 (2011) 1977–1984.
[6] J. Ding, N. Song, Z. Li, Synthesis, characterization and photovoltaic applications of a low band gap polymer based on s-tetrazine and dithienosilole, Chem. Commun. 46 (2010) 8668–8670.
[7] Z. Li, J. Ding, N. Song, J. Lu, Y. Tao, Development of a new s-tetrazine-based copolymer for efficient solar cells, J. Am. Chem. Soc. 132 (2010) 13160–13161.
[8] W. Kaim, The coordination chemistry of 1,2,4,5-tetrazines, Coord. Chem. Rev. 230 (2002) 127–139.
[9] W. Kaim, S. Berger, S. Greulich, R. Reinhardt, J. Fiedler, Electronic coupling of two [Cp*ClM](+)/[Cp*M] reaction centers via pi conjugated bridging ligands: similarities and differences between rhodium and iridium analogues, J. Organomet. Chem. 582 (1999) 153–159.
[10] K. Parimal, E.H. Witlicki, A.H. Flood, Interconverting two classes of architectures by reduction of a self-sorting mixture, Angew. Chem. Int. Ed. 49 (2010) 4628–4632.
[11] Y.H. Gong, P. Audebert, G. Clavier, F. Miomandre, J. Tang, S. Badre, R. Mealllet-Renault, E. Naidus, Preparation and physicochemical studies of new multiple rings s-tetrazines, New J. Chem. 32 (2008) 1235–1242.
[12] G.H. Spencer, P.C. Cross, K.B. Wiberg, s-Tetrazine. I. High-resolution vapor-phase study of the visible n–pi vibronic absorption band systems, J. Chem. Phys. 35 (1961) 1925–1938.
[13] G.H. Spencer, P.C. Cross, K.B. Wiberg, s-Tetrazine. II. Infrared spectra, J. Chem. Phys. 35 (1961) 1939–1945.
[14] S. Ghosh, M. Chowdhury, S1(n,π^*), T1(n,π^*) and S2(n,π^*) emissions in 3,6-diphenyl-s-tetrazine, Chem. Phys. Lett. 85 (1982) 233–238.
[15] R.M. Hochstrasser, D.S. King, Isotopically selective photochemistry in molecular-crystals, J. Am. Chem. Soc. 97 (1975) 4760–4762.
[16] R.M. Hochstrasser, D.S. King, Isotopically selective spectroscopy and photochemistry of sigma-tetrazine in crystals and mixed crystals at low-temperature, J. Am. Chem. Soc. 98 (1976) 5443–5450.
[17] R.M. Hochstrasser, D.S. King, A.C. Nelson, Subnanosecond dynamics of fluorescence and singlet absorption of s-tetrazine, Chem. Phys. Lett. 42 (1976) 8–12.
[18] R.M. Hochstrasser, D.S. King, A.B. Smith, Spectroscopy, photophysics, and photochemistry of dimethyl-s-tetrazine and phenyl-s-tetrazine in crystals and mixed-crystals at low-temperatures, J. Am. Chem. Soc. 99 (1977) 3923–3933.
[19] R. Métivier, F. Nolde, K. Müllen, T. Basché, Electronic excitation energy transfer between two single molecules embedded in a polymer host, Phys. Rev. Lett. 98 (2007) 047802.
[20] T.M. Wilson, M.J. Tauber, M.R. Wasielewski, Toward an n-type molecular wire: electron hopping within linearly linked perylenediimide oligomers, J. Am. Chem. Soc. 131 (2009) 8952–8957.
[21] J. Spanget-Larsen, E.W. Thulstrup, J. Waluk, Electronic states of diphenyl- and dipyridyl-s-tetrazines: linear and magnetic circular dichroism, and quantum chemical calculations, Chem. Phys. 254 (2000) 135–149.
[22] N.O. Abdel-Rahman, M.A. Kira, M.N. Tolba, A direct synthesis of dihydrotetrazines, Tetrahedron Lett. 9 (1968) 3871–3872.
[23] N.A. Ahmed, A.I. Kitaigorodsky, Experimental and theoretical determination of the crystal structure of 3,6-diphenyl-s-tetrazine, Acta Crystallogr. Sect. B 28 (1972) 739–742.
[24] M.J. Frisch, G.W., Trucks, H.B., Schlegel, G.E., Scuseria, M.A., Robb, J.R., Cheeseman, G., Scalmani, V., Barone, B., Mennucci, G.A., Petersson, H., Nakatsuji, M., Caricato, X., Li, H.P., Hratchian, A.F., Izmaylov, J., Bloino, G., Zheng, J.L., Sonnenberg, M., Hada, M., Ehara, K., Toyota, R., Fukuda, J., Hasegawa, M., Ishida, T., Nakajima, Y., Honda, O., Kitao, H., Nakai, T., Vreven, J. J. A. Montgomery, J.E., Peralta, F., Ogliaro, M., Bearpark, J.J., Heyd, E., Brothers, K.N., Kudin, V.N., Staroverov, R., Kobayashi, J., Normand, K., Raghavachari, A., Rendell, J.C., Burant, S.S., Iyengar, J., Tomasi, M., Cossi, N., Rega, J.M., Millam, M., Klene, J.E., Knox, J.B., Cross, V., Bakken, C., Adamo, J., Jaramillo, R., Gomperts, R.E., Stratmann, O., Yazyev, A.J., Austin, R., Cammi, C., Pomelli, J.W., Ochterski, R.L., Martin, K., Morokuma, V.G., Zakrzewski, G.A., Voth, P., Salvador, J.J., Dannenberg, S., Dapprich, A. D. Daniels, O., Farkas, J.B., Foresman, J.V., Ortiz, J., Cioslowski, D.J. Fox, Gaussian 09, Revision A.02, Gaussian, Inc., Wallingford CT, 2009.
[25] W.E. Ford, P.V. Kamat, Photochemistry of 3,4,9,10-perylenetetracarboxylic dianhydride dyes. 3. Singlet and triplet excited-state properties of the bis(2,5-di-tert-butylphenyl)imide derivative, J. Phys. Chem. 91 (1987) 6373–6380.
[26] S.I. van Dijk, P.G. Wiering, C.P. Groen, A.M. Brouwer, J.W. Verhoeven, W. Schuddeboom, J.M. Warman, Solvent-dependent switching between two dipolar excited-states in a rigidly extended trichromophoric system, J. Chem. Soc. Faraday Trans. 91 (1995) 2107–2114.
[27] J. Baffreau, S. Leroy-Lhez, N. Van Anh, R.M. Williams, P. Hudhomme, Fullerene C-60-perylene-3,4: 9,10-bis(dicarboximide) light-harvesting dyads: spacer-length and bay-substituent effects on intramolecular singlet and triplet energy transfer, Chem. Eur. J. 14 (2008) 4974–4992.
[28] K.M. Mullen, I.H.M. van Stokkum, TIMP: an R package for modeling multi-way spectroscopic measurements, J. Stat. Softw. 18 (2007).
[29] J. Ma, D. VanDenBout, M. Berg, Transient hole burning of s-tetrazine in propylene carbonate: a comparison of mechanical and dielectric theories of solvation, J. Chem. Phys. 103 (1995) 9146–9160.
[30] E. Kurach, D. Djurado, J. Rimarcik, A. Kornet, M. Wlostowski, V. Lukes, J. Pecaut, M. Zagorska, A. Pron, Effect of substituents on redox, spectroscopic and structural properties of conjugated diaryltetrazines—a combined experimental and theoretical study, Phys. Chem. Chem. Phys. 13 (2011) 2690–2700.
[31] Y.H. Gong, F. Miomandre, R. Méallet-Renault, S. Badre, L. Galmiche, J. Tang, P. Audebert, G. Clavier, Synthesis and physical chemistry of s-tetrazines: which ones are fluorescent and why? Eur. J. Org. Chem. (2009) 6121–6128.
[32] S.J. Strickler, R.A. Berg, Relationship between absorption intensity and fluorescence lifetime of molecules, J. Chem. Phys. 37 (1962) 814–822.
[33] R. Englman, J. Jortner, The energy gap law for radiationless transitions in large molecules, Mol. Phys. 18 (1970) 145–164.
[34] N.J. Turro, V. Ramamurthy, W. Cherry, W. Farneth, Effect of wavelength on organic photoreactions in solution—reactions from upper excited-states, Chem. Rev. 78 (1978) 125–145.
[35] S. Murata, C. Iwanaga, T. Toda, H. Kokubun, Fluorescence and radiationless transitions from the second excited states of azulene derivatives, Ber. Bunsen-Ges. Phys. Chem. 76 (1972) 1176–1183.
[36] B.D. Wagner, D. Tittelbach-Helmrich, R.P. Steer, Radiationless decay of the S_2 states of azulene and related-compounds—solvent dependence and the energy-gap law, J. Phys. Chem. 96 (1992) 7904–7908.
[37] G. Eber, S. Schneider, F. Dorr, Importance of intersystem crossing for deactivation of S_2 state of halogeno derivatives of azulene, Chem. Phys. Lett. 52 (1977) 59–62.
[38] G.G. Aloisi, F. Elisei, L. Latterini, G. Marconi, U. Mazzucato, Involvement of the upper excited state S-2 in the photophysics of trans-1,2-diarylethenes due to slow internal conversion to S-1, J. Photochem. Photobiol. A 105 (1997) 289–295.
[39] N. Kobayashi, H. Lam, W.A. Nevin, P. Janda, C.C. Leznoff, T. Koyama, A. Monden, H. Shirai, Synthesis, spectroscopy, electrochemistry, spectroelectrochemistry, Langmuir–Blodgett film formation, and molecular orbital calculations of planar binuclear phthalocyanines, J. Am. Chem. Soc. 116 (1994) 879–890.
[40] J.A. Mondal, H.N. Ghosh, T. Mukherjee, D.K. Palit, S_2 fluorescence and ultrafast relaxation dynamics of the S_2 and S_1 states of a ketocyanine dye, J. Phys. Chem. A 109 (2005) 6836–6846.
[41] J.A. Mondal, H.N. Ghosh, T. Mukherjee, D.K. Palit, Ultrafast relaxation dynamics of the excited states of Michler's thione, J. Phys. Chem. A 110 (2006) 12103–12112.
[42] G.G. Gurzadyan, T.H. Tran-Thi, T. Gustavsson, Time-resolved fluorescence spectroscopy of high-lying electronic states of Zn-tetraphenylporphyrin, J. Chem. Phys. 108 (1998) 385–388.